Solar Physics (2006) 237: 45–59
DOI: 10.1007/s11207-006-0077-6

CORRELATION BETWEEN SOLAR FLARE PRODUCTIVITY AND PHOTOSPHERIC MAGNETIC FIELD PROPERTIES

1. Maximum Horizontal Gradient, Length of Neutral Line, Number of Singular Points

YANMEI CUI, RONG LI, LIYUN ZHANG, YULIN HE, and HUANING WANG
National Astronomical Observatories, Chinese Academy of Sciences, Beijing 100012, China
(e-mail: ymcui@bao.ac.cn)

(Received 27 September 2005; accepted 31 May 2006; Published online 11 July 2006)

Abstract. From a large number of SOHO/MDI longitudinal magnetograms, three physical measures including the maximum horizontal gradient, the length of the neutral line, and the number of singular points are computed. These measures are used to describe photospheric magnetic field properties including nonpotentiality and complexity, which is believed to be closely related to solar flares. Our statistical results demonstrate that solar flare productivity increases with nonpotentiality and complexity. Furthermore, the relationship between the flare productivity and these measures can be well fitted with a sigmoid function. These results can be beneficial to future operational flare forecast models.

1. Introduction

Solar flares are very important events in the solar atmosphere. They explosively release large amount of energy in the form of electromagnetic emissions and particle acceleration, which may influence performance and reliability of space-borne and ground-based technological systems and can even endanger human life or health. In order to guarantee the safety of human activities in space, solar flares have to be forecasted.

Most solar flare forecast models depend on the statistical relationship between flares and morphological evolution of sunspots (McIntosh, 1990; Gallagher, Moon, and Wang, 2002). This relationship has been employed for a long time and plays an important role in daily flare forecasting. Unfortunately, it cannot directly show us the physical connection between flares and magnetic field evolution. And moreover, the descriptions on morphological evolution may differ between forcasters.

Many authors have investigated physical relationship between flares and the properties of photospheric magnetic fields, such as rapidly emerging new magnetic flux (Martres *et al.*, 1968; Wang and Shi, 1993; Nitta *et al.*, 1996), strong magnetic shear (Hagyard and Rabin, 1986; Hagyard, 1988; Sakurai *et al.*, 1992; Wang *et al.*, 1994), reconfiguration of magnetic fields (Fontenla *et al.*, 1995; Wang, Qiu, and Zhang, 1998), and imbalance of magnetic flux (Shi and Wang, 1994; Wang *et al.*, 2002; Tian and Liu, 2003). Leka and Barnes (2003a,b) analyzed the relationship of flares with several photospheric magnetic properties including morphology, horizontal spatial gradient, vertical current, current helicity, twist, etc. However, these

studies may be unreliable because they are not based on a statistically significant sample.

Employing SOHO/MDI successive longitudinal magnetograms, we select a large number of active regions to study the relationship between solar flare productivity and multiple quantified physical measures which describe certain properties of the magnetic field including nonpotentiality and complexity.

In Section 2, the data and measures will be described. In Section 3, the statistical analysis will be shown. And finally, the conclusion and discussion will be given in Section 4.

2. Data and Measures

2.1. DATA

Information on the photospheric magnetic field is obtained from SOHO/MDI full disk longitudinal magnetograms which have a pixel size of $2''$ and a noise level of 20 G (Scherrer *et al.*, 1995). The time interval between successive magnetograms is 96 minutes. Figure 1a shows a magnetogram obtained on November 2, 1997. The data for X-ray flares are from GOES, downloaded from `http://www.ngdc.noaa.gov/stp/SOLAR/ftpsolarflares.html#xray`.

Active regions which satisfy the following two conditions are selected: (i) the production of at least one X-ray flare with magnitude $\geq$ C1.0; (ii) being located within 30° of solar disk center where projection effects can be negligible. When identifying active regions in MDI longitudinal magnetograms, we adopt active region location data for the SGD solar event reports and from the web `http://www.solarmonitor.org/index.php`. Active regions are sought during the time period April 15, 1996 to January 10, 2004. During this time there are some

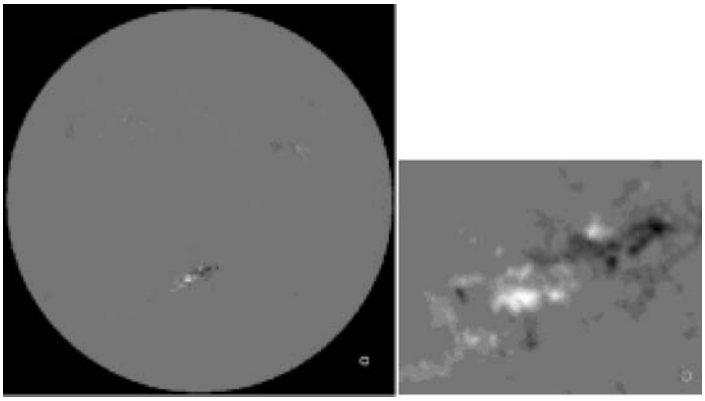

Figure 1. Full disk magnetogram and AR 8100 on November 2, 1997 (SOHO/MDI data).

gaps in MDI magnetograms due to defects in image processing of the spacecraft, especially at the beginning of the time period. The final number of active regions satisfying the above conditions in the present work is approximately 870, and the number of magnetograms containing these regions is 23 990. Our computational result indicates that these active regions appeared in the 23 990 maps 48 344 times. Figure 1b shows one of the active regions in a full disk magnetogram.

2.2. MEASURES

In order to quantitatively describe the properties of active region magnetic fields including nonpotentiality and complexity, three measures are employed: the maximum horizontal gradient ($|\nabla_{\rm h}\mathbf{B}_z|_m$), the length of the neutral line (L), and the number of singular points (η).

The horizontal gradient of the longitudinal magnetic field,

$$|\nabla_{\rm h}\mathbf{B}_z| = \left[\left(\frac{\vartheta \mathbf{B}_z}{\vartheta x}\right)^2 + \left(\frac{\vartheta \mathbf{B}_z}{\vartheta y}\right)^2\right]^{1/2}, \tag{1}$$

shows the nonpotentiality of active regions by specifying how magnetic fluxes are packed together, and generally connects with flare activity (McIntosh, 1990; Zirin and Wang, 1993; Zhang *et al.*, 1994; Gallagher, Moon, and Wang, 2002; Tian, Wang, and Wu, 2002; Leka and Barnes, 2003a). The maximum horizontal gradient $|\nabla_{\rm h}\mathbf{B}_z|_m$ indicates the maximum squeezing between two flux systems in an active region. Since the selected active regions are no farther than 30° of solar disk center, the difference between horizontal gradient and transverse gradient can be ignored.

The neutral line separates opposite polarities of longitudinal magnetic field. High gradient and strong shear usually appear in the vicinities of neutral lines, where flares frequently occur (Hagyard and Rabin, 1986; Zirin and Liggett, 1987; Hagyard, 1988; Zirin, 1988; Gary, Hagyard, and West, 1990; Wang *et al.*, 1994). Let L be the length of neutral line with a value of horizontal gradient larger than 0.041 G km^{-1} (60 G pixel^{-1}), which is triple the noise level in MDI magnetograms. For convenience, we employ the number of pixels along a neutral line to measure L (Falconer, 2001).

The topological structure of solar magnetic fields has been studied for a long time. Separatrices (surfaces that separate cells of different field line connectivities) and separators (the intersections of the separatrices) are believed to have close connections with magnetic reconnection and hence solar flares (Sweet, 1958, 1969; Baum *et al.*, 1979; Baum and Bratenahl, 1980; Gorbachev and Somov, 1988, 1989; Mandrini *et al.*, 1991, 1993; Démoulin *et al.*, 1993, 1994; Démoulin, Hénoux, and Mandrini, 1994; van Driel-Gesztelyi *et al.*, 1994; Wang and Wang, 1996; Wang, 1997; Zhang and Wang, 2002). Singular points are important for understanding the topological structures of solar magnetic fields because they are nodes in the

network formed by magnetic separatrices. Therefore, the number of singular points, η, suggests the complexity of topological structures.

The index of singular points in two dimensions can be described with Poincaré index, which is determined by the following formula:

$$I = \frac{1}{2\pi} \oint_L \frac{B_x B_y' - B_y B_x'}{B_y^2 + B_x^2} \mathrm{d}l, \tag{2}$$

where $B_x' = \frac{\mathrm{d}B_x}{\mathrm{d}l}$ and $B_y' = \frac{\mathrm{d}B_y}{\mathrm{d}l}$ (Arnold, 1973). Wang and Wang (1996) presented the definition of this index in detail and proposed a method for detecting two-dimensional magnetic singular points in a plane intersecting with magnetic fields. Here we briefly introduce this method and its applications. By taking the longitudinal magnetograms to be the boundary condition of a model potential field, we can compute the transverse component and also the two-dimensional singular points with index I in the transverse direction. The singular points with $I = +1$ correspond to concentrations of magnetic flux and those with $I = -1$ to the saddle points in the plane. There exists an uncertainty in determining η in quiet regions where the magnetic fields are below the noise level. In order to guarantee the reality of singular points detected, we take 200 G to be the threshold of the vector magnetic fields, which is larger than the assumed total noise level (20 G in the longitudinal magnetogram and 150 G in the transverse). Figure 2 shows that there are four points with $I = +1$ (denoted with "◯") and one point with $I = -1$ (denoted with "◇") in AR9574. Accordingly, the number of singular points is 5, *i.e.*, $\eta = 5$.

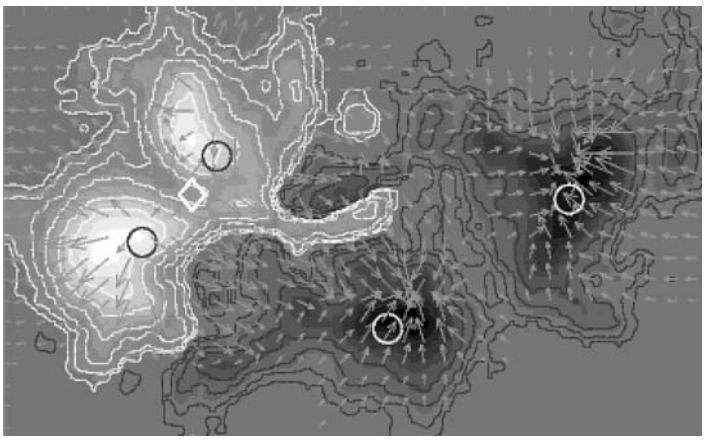

Figure 2. Two-dimensional singular points in AR9574 at 09:35:01 on August 11, 2001. The background is the gray map of longitudinal magnetic field with isogauss contours which levels are ±40, 80, 160, 320, 640, 960, 1280, 1600 G. The length of short bars is proportional to the transverse field, and the arrows show their directions. The four circles "◯" denote approximate positions of concentrations of magnetic flux; the diamond "◇" the position of saddle point. So, the number of singular points is 5.

Berger and Lites (2003) analyzed the calibration of MDI magnetograms, which may affect the computation for the magnetic measures. But these effects are too small to disturb the statistical results for the large number of samples, so we neglect that.

3. Statistical Analysis

The importance of solar flares is conventionally described with indexes of C, M, or X. Considering the selected active regions producing at least one C1.0 flare, we take C1.0 as the unit for measuring total X-ray importance. Within a certain time interval, the total importance, $\mathbf{I}_{\rm tot}$, is presented as,

$$\mathbf{I}_{\rm tot} = \sum C + 10 * \sum M + 100 * \sum X. \tag{3}$$

If an active region produces C1.2, C2.3, M4.1, and X1.2 flares within 48 hours, we have $\mathbf{I}_{\rm tot} = (1.2 + 2.3) + 10 * 4.1 + 100 * 1.2 = 164.5$.

An operational forecast model usually pays more attention to the production of flares with significance above a threshold within a given forward-looking period. Here, the threshold of $\mathbf{I}_{\rm tot}$ is supposed to be 10, *i.e.*, M1.0 equivalent. The forward-looking period is taken to be 48 hours, which is long enough for the evolution of photospheric magnetic fields.

3.1. Distribution of samples

In the total 48 344 samples, 8610 are associated with flares ($\mathbf{I}_{\rm tot} \geq 10$). We call them active samples.

By splitting the range of $|\nabla_{\rm h}\mathbf{B}_z|_m$ into eight equal-sized bins from 0 G km^{-1} to 0.8 G km^{-1}, the number of the total samples and the number of the active ones falling into each bin are counted, respectively. The rectangular histogram in Figure 3a shows two kinds of distributions, where the left y-axis represents the number of the total in each bin and the right axis the number of the active samples. From the difference between the two distributions, it can be seen that the active samples have a higher probability of falling into those bins with larger values than the total samples. This suggests that larger the maximum horizontal gradient, more frequently the solar flares occur. Similar results are also obtained from Figure 3b and c, which show the measures (L and η), respectively.

3.2. Flare productivity and magnetic field properties

The flare productivity is defined as

$$P(X) = S_{\rm a}(X)/S_{\rm t}(X), \tag{4}$$

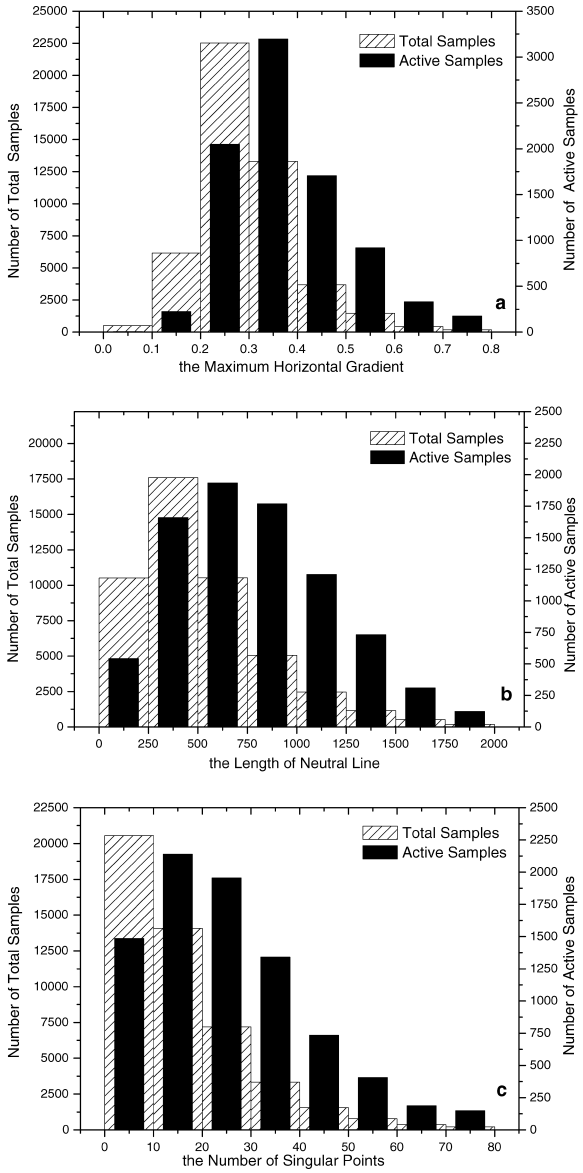

Figure 3. Distributions of the active samples and the total ones for the three measures ($|\nabla_{\mathrm{h}}\mathbf{B}_z|_m$, L and η).

where X is a random value of the three measures describing magnetic properties, $S_{\mathrm{a}}(X)$ and $S_{\mathrm{t}}(X)$ are the number of active samples and of the total when values of these measures are in the range $[X, \infty]$, respectively. For example, when the length of neutral line, L, is equal to or longer than 1200 pixels, there are 1701 active samples and 2573 total samples, and then the flare productivity, P, is 1701/2573 or 0.66.

In order to guarantee statistical efficiency, we do not calculate flare productivity when $S_t(X)$ is less than 500. Figure 4 shows the statistical relationship between the flare productivity and the measures. The distribution of data points in Figure 4a is sigmoid and therefore we fit them with a sigmoid function in Boltzmann style,

$$Y = A2 + \frac{A1 - A2}{1 + exp[(X - X0)/W]}, \tag{5}$$

where $A1$ and $A2$ are two asymptotic values that the function approaches but never quite reaches at small and large X; W is approximate width when the curve crosses over between $A1$ and $A2$ in a region of X values, which is centered around $X0$ (Marko, 2003). And, the slope of the curve is maximized at $X0$. Figure 4a exhibits this fitting curve and Table I gives the values of the corresponding fitting coefficients in Equation (5). The minimum and maximum flare productivity for the measure $|\nabla_h \mathbf{B}_z|_m$ are 0.164 and 0.738, respectively. When $X = 0.360\,\mathrm{G\,km^{-1}}$, the flare productivity has a remarkable increase. Maybe $0.360\,\mathrm{G\ km^{-1}}$ is the key point for producing solar flares in active regions.

The data points in Figure 4b and c show the relationship between the flare productivity and the other measures (L and η), which are more likely linear. It may be inferred that the points in Figure 4b and c are only distributed along the linear parts of sigmoid curves and the sigmoid function still can be employed to fit them. The fitting coefficients are also listed in Table I and the fitting curves are shown in Figure 4b and c. It should be pointed out that the goodness of fit (R^2) for the three curves is over 0.99, which suggests that the fitting function is reasonable. When $L = 763$ pixels or $\eta = 9$, the flare productivity also has a remarkable increase.

In addition, when $|\nabla_h \mathbf{B}_z|_m \approx 0.38\,\mathrm{G\,km^{-1}}$, $L \approx 850$ pixels, or $\eta \approx 34$, the flare productivity is about 0.5, and consequently these values may be the thresholds above which flares with an importance equal to or larger than M1.0 could occur in an active region within 48 hours.

3.3. Projection effects

For testing projection effects on our statistical results, we divide total samples into three groups according to their distances, D, from the central meridian. D satisfies the following inequalities for these three groups:

$$|D| \leq 10^\circ, \tag{6}$$

$$10^\circ < |D| \leq 20^\circ, \tag{7}$$

$$20^\circ < |D| \leq 30^\circ, \tag{8}$$

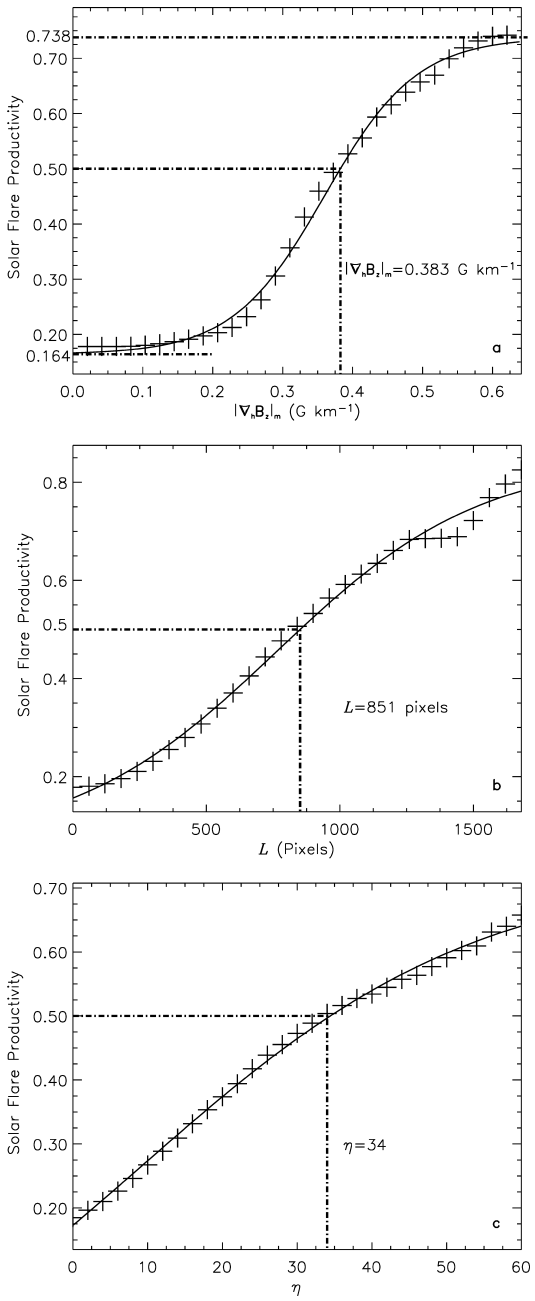

Figure 4. Flare productivity for each measure ('+' denotes the data points representing the flare productivity when X is equal to some values; the line is the Boltzmann sigmoidal fitting curve for these points).

TABLE I

Fitting coefficients in the sigmoid function and *goodness of fit* R^2 for each measure with a certain total importance threshold in a corresponding time window.

Total importance level	Time window (h)	Measure	$A1$	$A2$	$X0$	W	R^2
C5.0	48	$\|\nabla_h \mathbf{B}_z\|_m$	0.248	0.805	0.340	0.064	0.996
		L	0.110	0.883	617.66	381.60	0.990
		η	−0.125	0.758	4.847	19.250	0.999
M1.0	12	$\|\nabla_h \mathbf{B}_z\|_m$	0.054	0.344	0.366	0.057	0.997
		L	−0.071	2.159	2583.3	887.79	0.997
		η	−0.004	0.327	22.400	14.745	0.998
	24	$\|\nabla_h \mathbf{B}_z\|_m$	0.098	0.545	0.363	0.059	0.998
		L	−0.103	1.133	1283.8	738.75	0.995
		η	−0.048	0.514	17.583	17.099	0.996
	48	$\|\nabla_h \mathbf{B}_z\|_m$	0.164	0.738	0.360	0.066	0.996
		L	0.062	0.848	763.08	382.97	0.993
		η	−0.196	0.730	9.343	22.663	0.997
	72	$\|\nabla_h \mathbf{B}_z\|_m$	0.221	0.765	0.346	0.061	0.996
		L	0.153	0.852	695.36	301.66	0.997
		η	−0.074	0.775	11.202	19.310	0.998
M5.0	48	$\|\nabla_h \mathbf{B}_z\|_m$	0.035	0.493	0.428	0.080	0.997
		L	0.007	0.644	1180.8	391.00	0.998
		η	−0.007	0.311	22.750	13.491	0.996
X1.0	48	$\|\nabla_h \mathbf{B}_z\|_m$	0.017	0.411	0.468	0.088	0.996
		L	0.003	0.969	1730.3	438.78	0.999
		η	−0.105	0.771	74.236	41.480	0.996

respectively. The deviation between total samples and these three groups can be described by σ, which is defined as,

$$\sigma = \frac{\sum_i^N \left| P_{G_i} - P_{T_i} \right|}{N}, \tag{9}$$

where N is the number of data points for each measure in Figure 4, P_{G_i} is the flare productivity for a group, and accordingly P_{T_i} for total samples. Table II lists all values of σ for each group. Since the largest value of σ is not over 0.05, the deviation caused by projection effects can be ignored.

3.4. Flare productivity for different total importance thresholds

We can get different flare productivities by choosing different values of I_{tot} as thresholds to forecast flares in a 48 hours period. Figure 5 shows the statistical

TABLE II

Deviations, σ, between total samples and three groups. D represents the sample's distances from the central meridian.

σ	$\lvert\nabla_{\rm h}\mathbf{B}_z\rvert_m$	L	η
$\lvert D\rvert \leq 10^\circ$	0.031	0.025	0.029
$10^\circ < \lvert D\rvert \leq 20^\circ$	0.017	0.006	0.014
$20^\circ < \lvert D\rvert \leq 30^\circ$	0.037	0.040	0.041

results when the values of the threshold are set at 5 (C5.0), 10 (M1.0), 50 (M5.0), and 100 (X1.0), respectively. Table I also gives the fitting coefficients. Within the same period, the productivity of flares with high thresholds such as M5.0 and X1.0 is smaller than that of flares with low thresholds such as C5.0 and M1.0. This fact indicates that a large amount of free energy is not easily stored even in active regions with high nonpotentiality or high complexity.

3.5. Flare productivity in different time windows

Figure 6 shows the fitted curves of flare productivity versus measures ($|\nabla_{\rm h}\mathbf{B}_z|_m$, L, η) with an M1.0 threshold for various forward-looking time periods. The fitting coefficients are given in Table I. For each of the measures, a high flare productivity is connected with a long forward-looking period. This result seems reasonable because flares are more easily triggered by random disturbances in a longer time window.

Now, we have the relationships between solar flare productivity and magnetic field properties, which are well fitted with sigmoid functions. According to our statistical results, measures describing magnetic field nonpotentiality and complexity can be used to evaluate activity levels of active regions and offer information about the probability of producing flares. In addition, these measures can be employed to set up an operational flare forecast model supported by artificial intelligence techniques in which sigmoid functions are widely used.

3.6. Correlations among measures

Figure 7 shows the correlation among the three measures. The correlative coefficients are 0.58 between $|\nabla_{\rm h}\mathbf{B}_z|_m$ and L, 0.85 between η and L, and 0.54 between η and $|\nabla_{\rm h}\mathbf{B}_z|_m$. Although these measures represent different magnetic properties, they may be associated with the same MHD processes. For instance, newly emerging fluxes make the magnetic topological structure more complex, which causes an increase in the number of singular points. Meanwhile, the total length of the neutral line would grow due to new flux regions often appearing in the opposite polarity

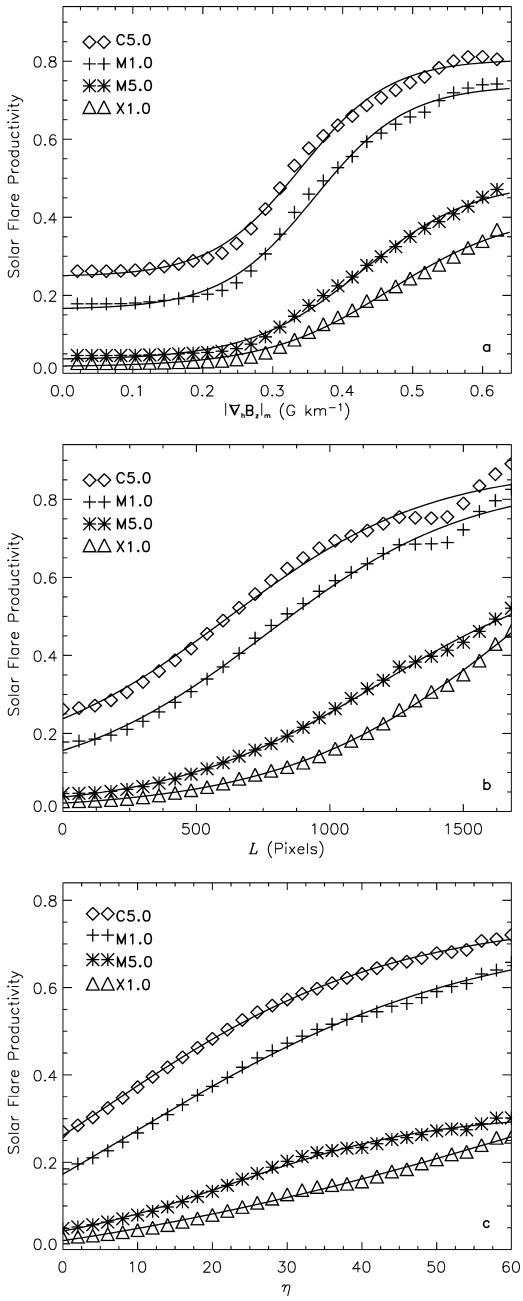

Figure 5. Relationship between flare productivity and the three measures ($|\nabla_h \mathbf{B}_z|_m$, L, η) when the thresholds of total flare importance are equal to 5 (C5.0), 10 (M1.0), 50 (M5.0), and 100 (X1.0). The lines are Boltzmann sigmoidal fitting curves to the data points.

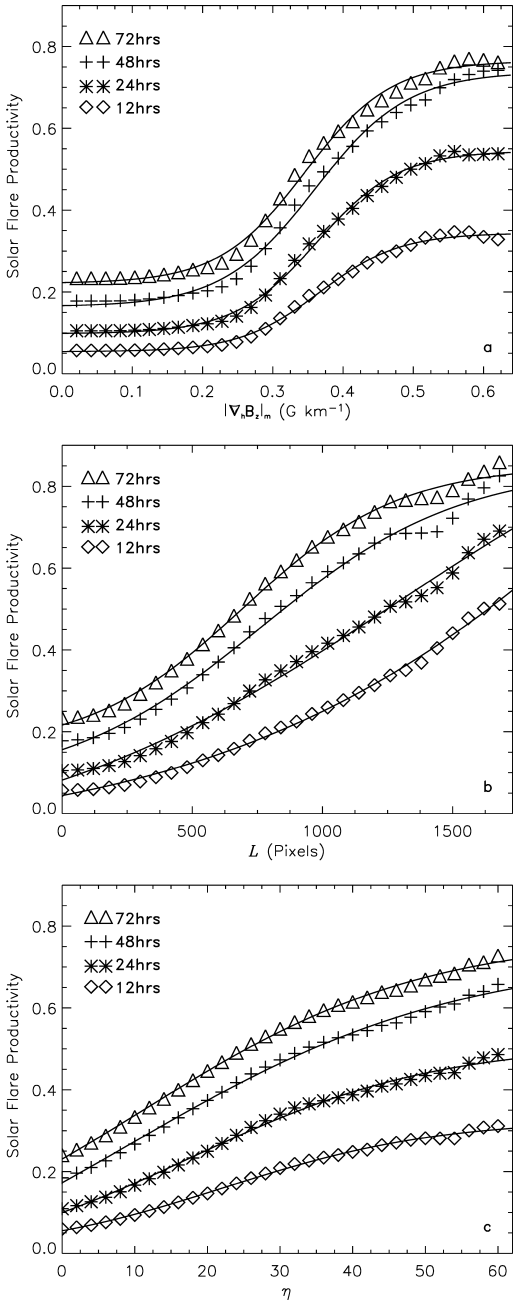

Figure 6. Relationship between flare productivity and the three measures ($|\nabla_{\rm h}\mathbf{B}_z|_m, L, \eta$) within different forward-looking periods. The lines are Boltzmann sigmoidal fitting curves to the data points.

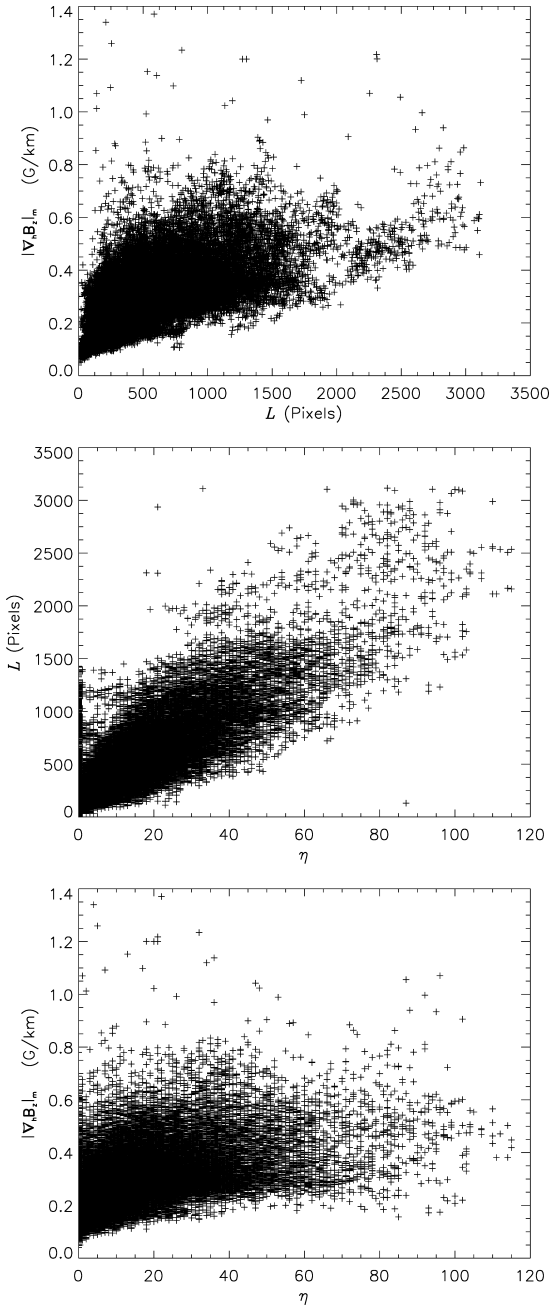

Figure 7. Correlation between these three measures ($|\nabla_h \mathbf{B}_z|_m$, L, η).

regions; the very strong gradient would also be likely produced by the collision of pre-existing fluxes and the new ones.

4. Conclusion and Discussion

From the above statistical results based on a large number of samples, we obtain the following conclusions:

1. Solar flare productivity closely connects with the three measures including the maximum horizontal gradient in longitudinal magnetograms, the length of the neutral line and the number of singular points, which increases with magnetic nonpotentiality or complexity;
2. The relationships between the flare productivity and magnetic properties can be well fitted with sigmoid functions.

However, none of these measures can absolutely determine whether solar flares would occur or not. It is possible to distinguish between an event-imminent photospheric magnetic state and an event-quiet state only by considering multiple measures simultaneously (Leka and Barnes, 2003b). Up to now, we have not considered other magnetic measures owing to the following two reasons. First, automatic processing of some measures is limited for a large number of samples; the other is the data of SOHO/MDI cannot offer transverse components of solar magnetic field. In the future work, the vector magnetograms observed at Huairou Solar Observing Station (HSOS) will be processed and some new measures will be obtained. Based on these measures, an operational flare forecast model will be set up by applying artificial intelligence techniques, such as artificial neural network (ANN) or support vector machine (SVM).

Acknowledgements

This work is supported by Chinese Academy of Sciences through grand KGCX2-SW-408 and National Natural Science Foundation of China (NSFC) under grant 10233050. The authors are indebted to the anonymous referees for helpful suggestions and the GOES and SOHO teams for providing the useful data.

References

Arnold, V.I.: 1973, *Ordinary Differential Equations*, MIT, Cambridge, Massachusetts.
Baum, P.J. and Bratenahl, A.: 1980, *Solar Phys.* **67**, 245.
Baum, P.J., Bratenahl, A., Crockett, G., and Kamin, G.: 1979, *Solar Phys.* **62**, 53.
Berger, T.E. and Lites, B.W.: 2003, *Solar Phys.* **213**, 213.

Démoulin, P., Hénoux, J.C. , and Mandrini, C.H.: 1994, *Astron. Astrophys.* **285**, 1023.
Démoulin, P., van Driel-Gesztelyi, L., Schmieder, B., Hénoux, J.C., Csepura, G., and Hagyard , M.J.: 1993, *Astron. Astrophys.* **271**, 292.
Démoulin, P., Mandrini, C.H., Hénoux, J.C., and Machado, M.E.: 1994, *Solar Phys.* **150**, 221.
Falconer, D.A.: 2001, *J. Geophys. Res.* **106**, 25185.
Fontenla, J., Ambasta, A., Kalman, B., and Csepura, G.: 1995, *Astrophys. J.* **440**, 894.
Gallagher, P.T., Moon, Y.-J., and Wang, H.: 2002, *Solar Phys.* **209**, 171.
Gary, G.A., Hagyard, M.J., and West, E.A.: 1990, *Solar Polarimetry, Proceedings of the Workshop on Solar Polarimetry*, National Solar Observatory, Sunspot, NM, p. 65.
Gorbachev, V.S. and Somov, B.B.: 1988, *Solar Phys.* **117**, 77.
Gorbachev, V.S. and Somov, B.B.: 1989, *Soviet Astron.* **33**(1), 57.
Hagyard, M.J.: 1988, *Solar Phys.* **115**, 107.
Hagyard, M.J. and Rabin, D.M.: 1986, *Adv. Space Res.* **6**, 7.
Leka, K.D. and Barnes, G.: 2003a, *Astrophys. J.* **595**, 1277.
Leka, K.D. and Barnes, G.: 2003b, *Astrophys. J.* **595**, 1296.
Mandrini, C.H., Démoulin, P., Hénoux, J.C., and Machado, M.E.: 1991, *Astron. Astrophys.* **250**, 541.
Mandrini, C.H., Rovira, M.G., Démoulin, P., Hénoux, J.C., Machado, M.E., and Wilkinson, L.K.: 1993, *Astron. Astrophys.* **272**, 609.
Marko, L.: 2003, *Ind. Phys.* **9**(2), 24.
McIntosh, P.S.: 1990, *Solar Phys.* **125**, 251.
Martres, M.-J., Michard, R., Soru-Iscovici, I., and Tsap, T.T.: 1968, *Solar Phys.* **5**, 187.
Nitta, N., van Driel-Gesztelyi, L., Leka, K.D., and Shibata, K.: 1996, *Adv. Space Res.* **17**, 201.
Sakurai, T., Shibata, K., Ichimoto, K., Tsuneta, S., and Acton, L.W.: 1992, *Publ. Astron. Soc. Jpn.* **44**, L123.
Scherrer, P.H., Bogart, R.S., Bush, R.I., Hoeksema, J.T., Kosovichev, A.G., Schou, J., *et al.*: 1995, *Sol.Phys.* **162**, 129.
Shi, Z. and Wang, J.: 1994, *Astrophys. J.* **149**, 105.
Sweet, P.A.: 1958, *Nuovo Cimento Suppl. Ser. X* **8**, 188.
Sweet, P.A.: 1969, *Ann. Rev. Astron. Astrophys.* **7**, 149.
Tian, L. and Liu, Y.: 2003, *Astron. Astrophys.* **406**, 337.
Tian, L., Wang, J., and Wu, D.: 2002, *Solar Phys.* **209**, 375.
van Driel-Gesztelyi, L., Hofmann, A., Démoulin, P., Schmieder, B., and Csepura, G.: 1994, *Solar Phys.* **149**, 309.
Wang, H.N.: 1997, *Solar Phys.* **174**, 265.
Wang, H., Ewell, M.W., Jr., Zirin, H., and Ai, G.: 1994, *Astrophys. J.* **424**, 436.
Wang, T., Qiu, J., and Zhang, H.: 1998, *Astron. Astrophys.* **336**, 359.
Wang, H., Spirock, T.J., Qiu, J., Ji, H., Yurchyshyn, V., Moon, Y.-J., *et al.*: 2002, *Astrophys. J.* **576**, 497.
Wang, J. and Shi, Z.: 1993, *Solar Phys.* **209**, 375.
Wang, H.N. and Wang, J.: 1996, *Astron. Astrophys.* **313**, 285.
Zhang, H., Ai, G., Yan, X., Li, W., and Liu, Y.: 1994, *Astrophys. J.* **423**, 828.
Zhang, C.X. and Wang, J.: 2002, *Solar Phys.* **205**, 303.
Zirin, H.: 1988, *Astrophysics of the Sun*, Cambridge University Press, Cambridge.
Zirin, H. and Liggett, M.A.: 1987, *Solar Phys.* **113**, 267.
Zirin, H. and Wang, H.: 1993, *Solar Phys.* **144**, 37.